NUMERICAL MODEL AND AN ANALYSIS OF INERTIAL ACCUMULATOR OPERATION UNDER SELECTED WORKING CONDITIONS

Mateusz KUKLA*, Maksymilian RACHEL*

*Faculty of Mechanical Engineering, Poznan University of Technology, ul. Piotrowo 3, 61-138 Poznan, Poland

mateusz.kukla@put.poznan.pl, maksymilian.rachel@student.put.poznan.pl

received 22 May 2022, revised 21 August 2022, accepted 22 August 2022

Abstract: The aim of this paper was to create a computational model that will enable the evaluation of the operation of a conventional inertia accumulator. This is an issue that is relevant as storage of energy is becoming increasingly important, in particular when it comes to generating electricity from renewable sources. In the course of the conducted works, an analytical model was developed based on the available literature, and then, it was introduced into the environment for numerical calculations. Four variants resulting from different geometrical parameters of the flywheel were adopted successively. On this basis, a series of simulations were performed, which allowed for obtaining the characteristics of the analysed solutions. As a consequence, a number of characteristics related to the mechanical power and energy of the simulated kinetic energy accumulators were obtained. The test results therefore provide a basis for comparing kinetic energy accumulators with different geometries and drive solutions.

Key words: mechanical energy accumulator, flywheel, inertial accumulator, numerical simulations, non-conventional technical solutions

1. INTRODUCTION

The generation of energy, in particular electric energy, using renewable sources is growing rapidly. This increase is expected to continue as it is associated with an overall increase in energy demand but also with progressive trends in reducing environmental impact [1]. Moreover, a significant decrease in the costs of generating energy from renewable sources has been observed in recent years [2], which additionally increases the demand.

Some of the methods of producing energy from renewable sources are characterised by a discontinuous nature of work. Examples include solar panels and wind farms that need sunlight and wind, respectively, in order to operate, which are not always adequately abundant. Moreover, the demand for electricity is also not constant and is characterised by periods of increased demand in cycles that may result from the time of the day or the season of the year. Since the production of energy from renewable sources is increasing, the inevitable interruptions in their operation of some of them make it necessary to have the capacity to store large amounts of energy in order to be able to meet the possible demand at any time [3]. Therefore, the legitimacy of developing energy storage systems can be indicated. An energy storage system allows electricity to be produced when needed and stored when energy generation exceeds demand. Energy storage is especially advantageous during low demand, low production cost period or interruptions in the continuity of available sources. Thanks to this, the stored energy reserve can be used in the event of high demand, increase in generation costs or the lack of availability of an alternative generation [4–6].

Among the energy storage systems, one can point out kinetic energy accumulators, which are an extension of the flywheel concept. The major advantage of inertial accumulators is the high power density [7]. It results from the very low achievable mass of the accumulator being maintained in compact construction. Furthermore, it is characterised by good overload resistance and low effect of temperature on correct operation. Its other advantages include low maintenance requirements and the possibility to determine the exact amount of stored energy by measuring rotation speed. In addition, they are resistant to cyclical degradation but also to deep discharges, which is typical for classic electrochemical batteries. Additionally, the efficiency of their cycle can reach values up to 95% [8, 9]. High charging and discharging rates, projected service life exceeding 20 years as well as specific energies that may exceed the value of 100 Wh/kg [10, 11] should also be considered favourable. Moreover, when the stored energy is converted into electricity, the fast response time of the inertial accumulators means that they are capable of balancing the grid frequency. It should be expected that as a result of the increase in the share of energy generated with the use of irregular energy sources, this feature will play an increasingly important role [15].

Its main disadvantage includes the very limited time of energy storage because the motion resistance of the inertial accumulator cannot be completely eliminated. Therefore, inertial accumulators are characterised by relatively average ratio of stored energy per unit of mass [13]. This is one of the main reasons for the limited application for kinetic energy accumulators. Another limitation is the type of stored energy. Electrical energy is much more versatile, and a large number of devices can be powered directly by it by utilising relatively simple systems with a very low number of mechanical components.

Despite their flaws, inertial accumulators can be employed in devices which do not operate in a continuous cycle, for example, which are engaged for a limited time or operate under variable load. The potential for their application involves fast transmission of large amounts of energy which is achievable due to high power

density of the inertial accumulators. Some of the current applications of kinetic energy accumulators include the following examples: stabilising satellites on an orbit [14], short-term energy storage from photovoltaic panels [15], recovery of brake energy in automobiles [16–18], trolleybus drives [19], etc.

The aim of the research was to create a computational model, thanks to which it will be possible to evaluate the work of a conventional inertial accumulator. To achieve this, an analytical model was developed based on the available literature and then introduced into the numerical computing environment. This allowed for a series of simulations and, as a result, the evaluation of the parameters of the modelled solution.

Within the scope of this work, a rotor fulfilling the requirements of a conventional inertial accumulator was analysed. It is a solid of revolution with a plane of symmetry perpendicular to the axis of rotation and height much lower than its radius. The material for the rotor is assumed construction steel grade 18G2A (S355J2); it is further assumed that the material characteristics are homogenous and isotropic. With the use of analytical calculations following a methodology provided in item [20], the rotor parameters were determined, based on allowable stress for the assumed material. These include the following: external radius r_z = 0.15 m, internal radius r_w = 0.018 m, height h = 0.018 m, moment of inertia J_B = 0.112 kg·m2, inertial accumulator mass m_B = 9.844 kg and maximum kinetic energy E_{max} = 61,411 J.

2. MATHEMATICAL MODEL

There are two sources of loss in kinetic energy accumulators. The first one results from friction in the bearing system. The other source is related to liquid viscosity (the gas filling the interior of the accumulator) in which the rotor is moving. To determine the approximate value of these losses, formulas used to determine the loss of power in discs and cylinders were employed [21]. The loss of energy occurring on the one side of the rotor disc N_T can be described with the following equation:

$$N_T = 1.96 \cdot 10^{-5} \rho_g C_T \omega^3 (d_z^5 - d_w^5) \text{ [kW]}, \quad (1)$$

where ρ_g is mass density of the gas (kg/m3), C_T is moment of friction indicator and d_z and d_w are, respectively, the external and internal diameter of the inertial accumulator (m). It was assumed that the inertial accumulator chamber will be filled with air with reduced pressure, maximum p = 0.3 bar, which is the upper threshold of the so-called low vacuum. Air density is calculated from the following equation:

$$\rho_g = \frac{pM_g}{RT_0}, \quad (2)$$

where M_g is molar mass of the gas (kg/mol), T_0 is gas temperature (K) and R = 8.314 (J/[kg·mol]) is universal gas constant. The molar mass for air is M_g = 0.029 kg/mole. Assuming average gas temperature as 40°C = 313.15 K, one can calculate the air density as the following value: ρ_g = 0.334 kg/m3. The next factor is the moment of friction coefficient C_T. It is calculated based on Reynolds number for the disc Re_T, the gap between the rotor and its enclosure s as well as the relative roughness of the rotor surface k. Assuming the gap size is s = 0.006 m and the fact that the manufactured disc roughness is Rz = 6.3 (Ra = 1.25), k = 6.3·10^{-6} m. Reynolds number Re_T is calculated based on the external radius of the inertial accumulator r_z, angular velocity ω and kinematic viscosity index ν_k, which is dependent on gas density ρ_g and dynamic viscosity μ (Pa·s). Gas density is calculated as above, whereas for air in temperature at 40°C, dynamic viscosity is equal to μ = 1.91·10^{-5} Pa·s. The kinematic viscosity is derived with the following equation:

$$\nu_k = \frac{\mu}{\rho_g}, \quad (3)$$

and is equal to ν_k = 5.72 · 10^{-5} m^2/s. Therefore, Reynolds number, calculated from the below equation:

$$Re_T = \frac{r_z^2 \omega}{\nu_k}, \quad (4)$$

is equal to Re_T = 411,923. Subject literature provides ranges of values for the Re_T with each one being assigned a respective equation to determine the moment of friction coefficient. The limit value between ranges is defined with the following equation:

$$Re_{gr} = 1{,}100 \left(\frac{r_z}{2k}\right)^{\frac{2}{5}} \cdot \left[3.8\, log\left(\frac{r_z}{2k}\right) - 2.4 \left(\frac{s}{r_z}\right)^{\frac{1}{4}}\right]. \quad (5)$$

After substituting the values and solving, the following is obtained: Re_{gr} = 676,828. Accordingly, the calculated Reynolds number is included in the third range (satisfying the inequality 10^5 < Re_T < Re_{gr}). Therefore, the index of friction may be determined from the equation:

$$C_T = 0.0102 \left(\frac{s}{r_z}\right)^{1/10} \cdot \frac{1}{Re_T^{\frac{1}{5}}}, \quad (6)$$

which allows to determine the value C_T = 5.57·10^{-4}. Considering the above, after solving Eq. (1), one arrives at $N_T \approx$ 0.01 kW.

Employing the limit values of the Reynolds number allows us to calculate the limit values of angular velocities for the third range, according to the following equation:

$$\omega_{gr} = \frac{Re_T}{Re_{gr}}, \quad (7)$$

Consequently, one obtains the minimum and maximum value of angular velocity: ω_{min} = 636.85 rad/s and ω_{max} = 4,310.35 rad/s, respectively.

Power losses on the side surface of the rotor are also dependent on the Reynolds number value Re_C, as in the equation:

$$Re_C = \frac{r_z \omega s}{\nu_k}, \quad (8)$$

and are equal to Re_C = 16,477. Analogous to the calculations involving the disc, the form of the loss equation is dependent on the range of the Reynolds number value Re_C. These are described with Taylor-Wendt equations. Since the inequality 1.6·10^4 < Re_C is true, therefore the power of the losses on the side surface of the rotor shall be described with the equation:

$$N_C = 2.3 \cdot 10^{-5} d_z^4 \omega^3 h \rho_g \sqrt{\frac{\nu_k}{r_z \omega s}}, \quad (9)$$

and for the discussed case shall be equal to $N_C \approx$ 0.01 kW. The total surface of the inertial accumulator is the sum of the upper and lower side surface as well as the side surface, which can be represented as follows:

$$N_B = 2N_T + N_C, \quad (10)$$

therefore, allowing to calculate N_B = 0.03 kW = 30 W.

Losses in bearings result from the friction between the rolling components and races. They are dependent on numerous factors,

DOI 10.2478/ama-2022-0034

including the lubrication method. The losses are determined approximately, based on the braking moment resulting from gravity. Its value is independent from rotational speed and can be calculated with the following equation:

$$M_{h1} = \frac{1}{2} m_B g f d. \tag{11}$$

Assuming the rolling resistance for steel of f = 0.016 and the diameter of the journal (depending on preliminary strength calculations) of d = 0.035 m, one arrives on: M_{h1} = 0.026 Nm. As per the subject literature [21], it is assumed to be the main source of braking moment in bearings and is therefore sufficient for the purpose of energy analysis.

Due to the high variance of the angular velocity during accumulator operation, it is efficient to express the total braking moment as:

$$M_h = c_1 \omega^2 + c_2, \tag{12}$$

where c_1 is a constant obtained after factoring out from the maximum aerodynamic loss Eq. (10) (the value ω^3) and c_2 = M_{h1} is constant moment of resistance in the bearings, according to Eq. (11). The values are c_1 = 2.64·10^{-8} kg·m^2 and c_2 = 0.026 Nm.

3. NUMERICAL CALCULATIONS

3.1. Numerical model

Numerical value determination is based on the power balance in the system expressed as follows:

$$N_{lad}(t) = N_{mag}(t) + N_{str}(t), \tag{13}$$

where $N_{str}(t)$ is the power of losses, which is the product of the moment M_h and the angular velocity of the rotor at a given moment $\omega(t)$, $N_{mag}(t)$ is power stored in the accumulator and $N_{lad}(t)$ is the power supplied to the inertial accumulator shaft. By substituting the equations established previously, the equation can be expressed as follows:

$$N_{lad}(t) = [J_B \dot{\omega}(t) + c_1 \omega^2(t) + c_2] \cdot \omega(t). \tag{14}$$

For the purpose of numerical calculations, a source of charging energy was assumed as a hypothetical electrical permanent magnet synchronous motor (PMSM). The characteristics of this motor are shown in Fig. 1.

This serves as a basis for deriving the three methods of charging the accumulator. Since the developed model is based on the flow of power, it is possible to charge the accumulator in the full variance range of speed and torque. However, this requires to utilise the correct type of variable ratio transmission. The present study does not account for losses of power occurring in such a transmission as the performed analysis focuses on the kinetic energy accumulator. The inertial accumulator charging time was selected to allow it to reach the maximum speed, i.e., where the maximum kinetic energy value is close to E_{max} = 61,411 J. For the motor, the following nominal parameter values were assumed: rotational speed n_0 = 8,000 rpm, torque M_0 ≈ 1.2 Nm and power N_0 ≈ 1 kW.

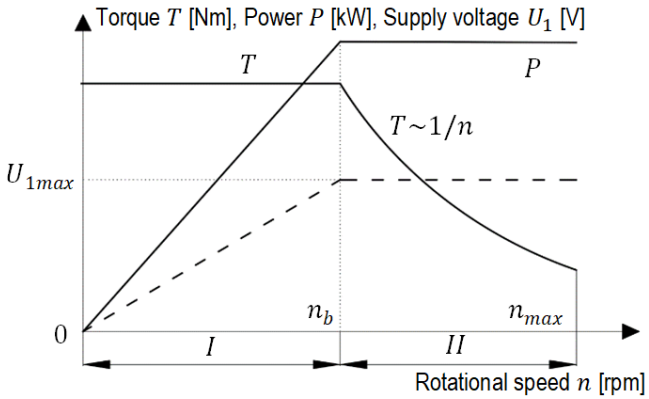

Fig. 1. PMSM drive characteristics. Below the nominal speed n_n, the drive operates with a constant torque of T (range I); after, it is exceeded, it operates at a constant power of P (range II), developed based on [20]

Based on the variance of rotational speed $n(t)$ and torque $M(t)$, the model calculates power supplied to the energy accumulator with the following equation:

$$N_{lad}(t) = \frac{M(t) n(t)}{9.55}. \tag{15}$$

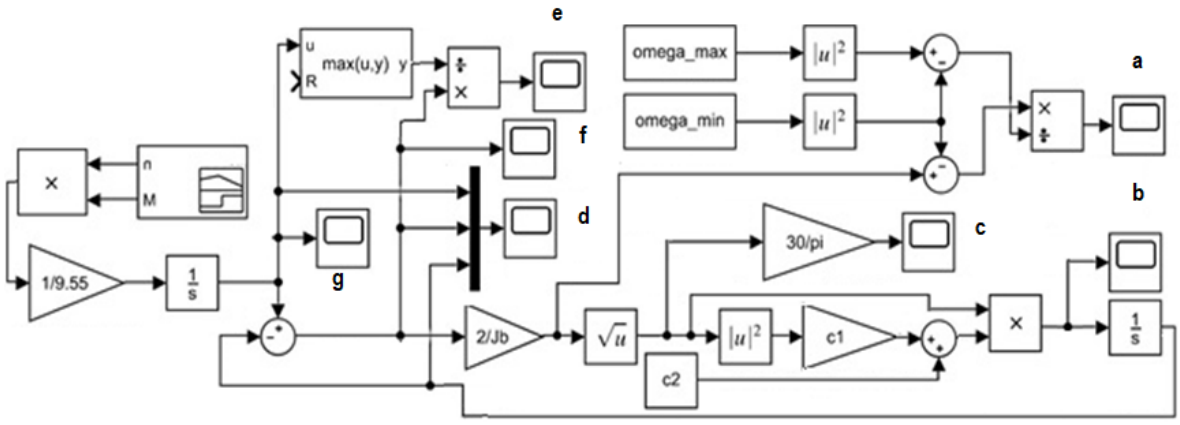

Fig. 2. Numerical calculations model diagram; a – charge degree, b – loss power, c – rotational speed, d – energy variance, e – efficiency, f – stored energy, g – charging energy (supplied by drive)

After integrating the calculated power, we arrive at the energy supplied to the accumulator $E_{lad}(t)$. However, the energy stored in the accumulator $E_{mag}(t)$ is expressed with the following equation:

$$E_{mag}(t) = E_{lad}(t) - E_{str}(t), \tag{16}$$

where is $E_{str}(t)$ is energy loss. Eq. (16) describes the value of $E_{mag}(t)$, which is also calculable from the kinetic energy equation. The equation can be transformed as follows:

$$\omega(t) = \sqrt{\frac{2E_{mag}(t)}{J_B}}. \tag{17}$$

Eq. (17) is employed to calculate the loss power $N_{str}(t)$; after integration, it allows us to calculate the loss energy $E_{str}(t)$. Additionally, accumulator efficiency ratio $\eta(t)$ was determined by referencing to energy stored in a given moment $E_{mag}(t)$ and the maximum value of supplied energy $E_{lad\,max}$. This can be expressed in the form of the following equation:

$$\eta(t) = \frac{E_{mag}(t)}{E_{lad\,max}} \cdot 100\%. \tag{18}$$

The charge of the accumulator can be expressed as an equation comprising the previously established values:

$$k(t) = \frac{\omega^2(t) - \omega_{min}^2}{\omega_{max}^2 - \omega_{min}^2} \tag{19}$$

MATLab Simulink software package was used to develop the previously defined model. It allows us to carry out simulations and make calculations in real time. The model view as developed in the software environment is provided in Fig. 2.

3.2. Numerical model

There are three states of accumulator operation: charge, discharge and self-discharge. When loading, the inertial accumulator accelerates to high speed due to the torque and velocity applied to the shaft. Analogously, during discharge, an external load is applied to the inertial accumulator shaft. During self-discharge, which usually is the longest of the states, the rotor shaft is decoupled and rotates freely. The speed of revolution at this point is close to nominal; the only load is affected by motion resistances and causes a slow reduction of speed [21]. Consequently, a simulation of operation of the modelled device was carried out for each described state of operation, resulting in three cases: C1, C2 and C3.

Tab. 1. Adopted properties and marking of individual rotors

Rotor marking	B1	B2	B3	B4
External radius r_z (m)	0.15	0.15	0.13	0.13
Internal radius r_w (m)	0.018	0.018	0.018	0.018
Height h (m)	0.018	0.015	0.018	0.02
Moment of inertia J_B (kg·m^2)	0.112	0.094	0.063	0.07
Mass m_B (kg)	9.844	8.203	7.358	8.176
Maximum kinetic energy E_{max} (J)	61,411	51,332	34,746	38,607
Constant c_1 (kg·m^2)	2.78 ·10^{-8}	2.5 ·10^{-8}	1.081 ·10^{-7}	1.191 ·10^{-7}
Constant c_2 (Nm)	0.027	0.02	0.016	0.018
Minimum value of angular velocity ω_{min} (rad/s)	636.82	636.82	516.38	516.38

In order to conduct the simulations, four variants of the analysed rotors were adopted. Apart from the rotor described in the previous chapters (marked as B1), calculations were also made for three other variants differing in radius r or height h. As they have different moments of inertia, the maximum kinetic energy for each of them varying charging times has been adopted. The dimensions and properties of selected variants are presented in Tab. 1.

As it can be seen from the presented description, 12 simulation variants were finally obtained, resulting from the combination of three charging methods (C1, C2 and C3) with four different rotors (B1, B2, B3 and B4).

4. RESULTS AND DISCUSSION

The first simulated scenario (Fig. 3) involves motor deceleration from the speed (n = 9,500 rpm). Since the motor operating range was at constant power, the initial torque was T = 1 Nm. It achieved the nominal value at speed n = 8,000 rpm and subsequently entered the stage of operation with constant torque until stopped. The entire operation took place over 108 s. The second scenario (Fig. 4) was performed with the motor operating under nominal conditions, i.e., with speed of n = 8,000 rpm and torque value of T = 1.2 Nm. This type of charging simulates a situation when the shaft (transmission) of the rotor is coupled with the motor without load. In this case, the acceleration took only 62 s. The third charging scenario (Fig. 5) involved an arrangement in which the accumulator is charged as the motor accelerates to achieve nominal operating conditions. This is by far the longest operation (120 s)

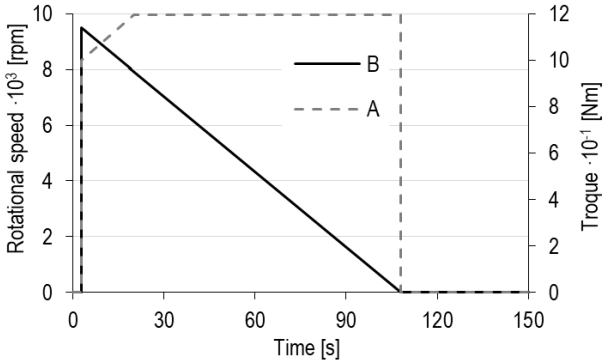

Fig. 3. Charging characteristics for the first scenario C1; A – torque, B – rotational speed

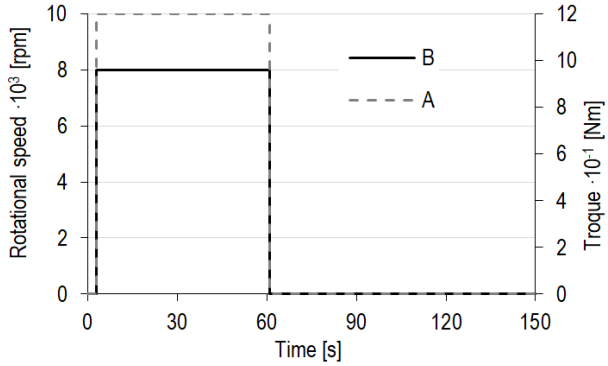

Fig. 4. Charging characteristics for the first scenario C1; A – torque, B – rotational speed

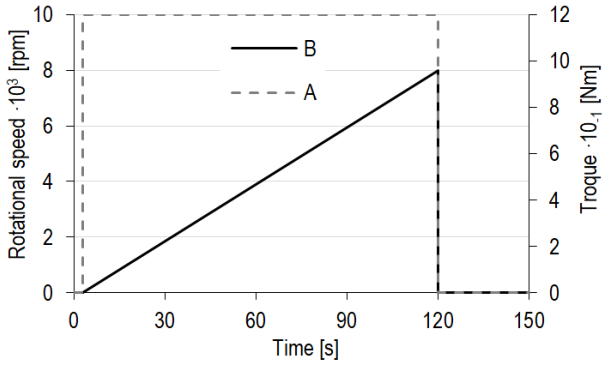

Fig. 5. Charging characteristics for the third scenario C3; A – torque, B – rotational

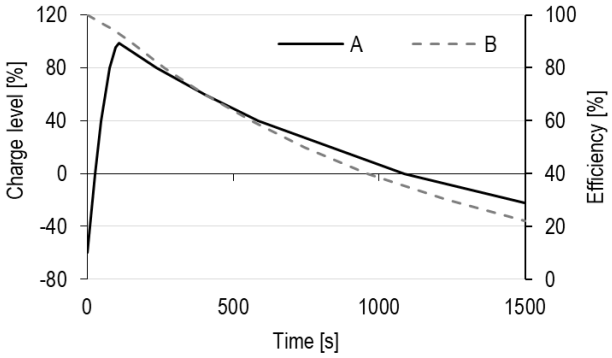

Fig. 6. Percentage variability graphs: A – charge level, B – efficiency

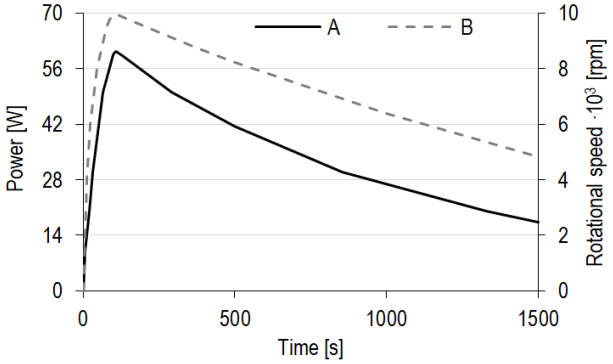

Fig. 7. Graph lines variability as a function of time: A – loss power, B – rotational speed

From the proposed group of variants, the rotors B1 and B2 should be considered the best because despite their slightly larger dimensions, they are able to accumulate almost twice as much energy as compared with rotors with smaller radii. Moreover, after about 5 min (300 s), they still have an energy of 4,000 J and a charge level of about 0.5. Ultimately, however, due to the greater energy capacity, it should be pointed out that the most effective solution is the rotor B1. Fig. 6 shows the degree of charge and efficiency of the system. Fig. 7 presents the variance in rotational speed of the rotor and power loss as a function of time.

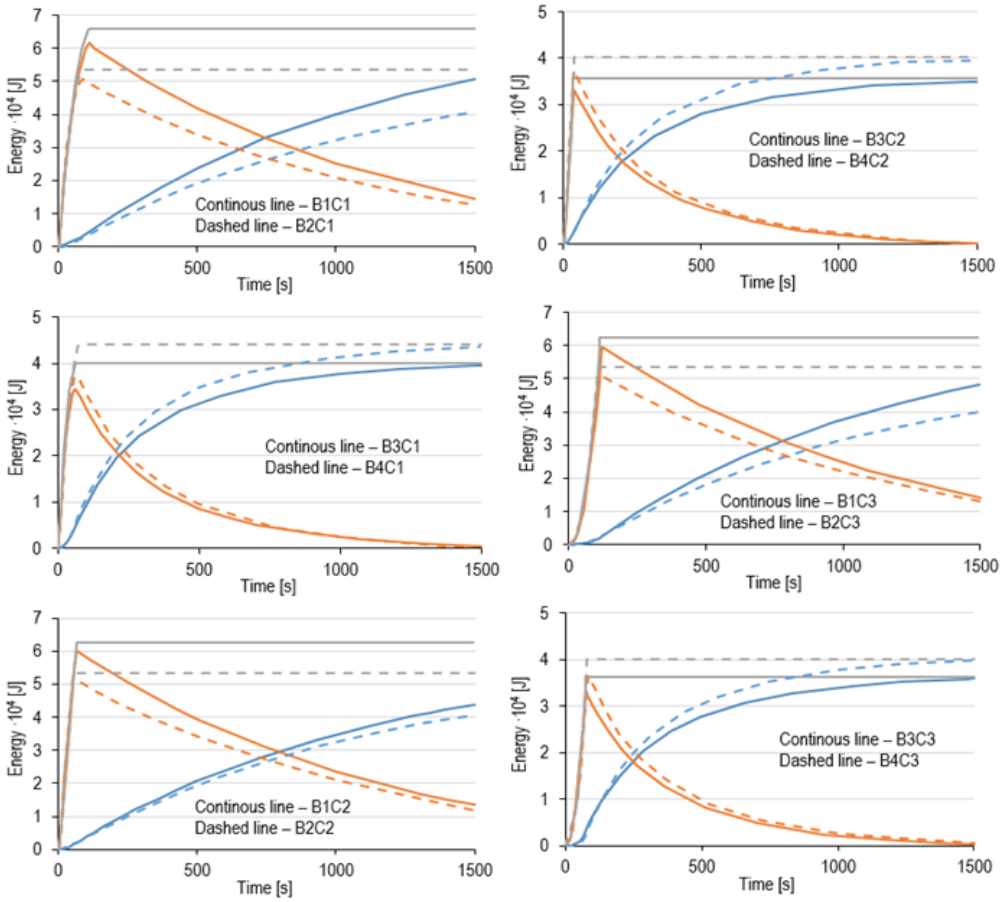

Fig. 8. Variance of energy as a function of time; blue lines represent energy loss, orange lines represent accumulated energy and gray lines represent charging energy; continuous and dashed lines represent different variants according to the legend

The graphs presented in Fig. 8 show the energy values in the system for different variants. It should be noted that the constants used in the model and the relationships on the basis of which they were determined rely on theoretical considerations and thus may not cover all the phenomena affecting the operation of the energy storing device or describe them only to a limited extent. The use of the charge level allows for a slightly more accurate reflection of the actual state of the accumulator capacity, due to the possible change in the value of the start power when operating at a speed lower than the minimum value of angular velocity.

The analysis of the presented graphs shows that the energy loss of the rotors B3 and B4 progresses much faster. This is due not only to the much lower maximum stored energy (more than by a half) but also to the much larger losses due to the smaller rotor diameter, which largely influenced the aerodynamic drag.

The different charging methods have little effect on the behaviour of the accumulator, except that charging with constant power is by far the shortest. The times for decreasing and increasing speeds are similar, and the difference is the result of the engine entering the state of work with constant power. However, it is worth bearing in mind that in the case of charging with a braking engine, the transition from the charging state to the self-discharging state is the smoothest, which in the case of a longer period of use may be important in terms of the durability of cooperating elements such as bearings.

5. SUMMARY

The analysis of presented data allows us to observe the operation of the modelled system. Based on the established graph lines, it is possible to determine that different charging methods do not materially affect the operation of the accumulator; on the other hand, charging time with constant power is by far the shortest. Charging times for acceleration and deceleration are similar, the difference being the result of the motor entering the state of operating under constant power. One should keep in mind that in the case of supplying energy to the system with decelerating motor, the transition from the charging state to self-discharging state is the smoothest. With longer times of operation, this may affect the durability of the mechanical system components, such as, bearings.

To summarise, the mathematical model was developed and implemented within the framework of software environment for numerical calculations. This allowed us to identify a series of graph lines and characteristics for the analysed system. The results of carried out works enable the comparison of different kinetic energy accumulators with different geometries and different methods of operation. Consequently, it is possible to develop the basis and a number of input data to be used in the design of this type of equipment.

REFERENCES

1. Chen H, Cong TN, Yang W, Tan C, Li Y, Ding Y. Progress in electrical energy storage system: A critical review. Prog Nat Sci. 2009;19:291–312.
2. Kåberger T. Progress of renewable electricity replacing fossil fuels. Global Energy Interconnection. 2018;1:48–52.
3. Moriarty P, Honnery D. Can renewable energy power the future? E Policy, 2016;93:3–7.
4. Medina P, Bizuayehu AW, Catalao JPS, Rodrigues EMG, Contreras J. Electrical Energy Storage Systems: Technologies' State-of-the-Art, Techno-economic Benefits and Applications Analysis. Proc of the 47th Hawaii Int Conf on Syst Sci; 2014 Jan 6–9; Waikoloa, HI, USA, 2014;2295–2304.
5. Hadjipaschalis I, Poullikkas A, Efthimiou V. Overview of current and future energy storage technologies for electric power applications. Renew Sust Energ Rev. 2009;13:1513–1522.
6. Del Granado PC, Wallace SW, Pang Z/The value of electricity storage in domestic homes: A smart grid perspective. E Systems, 2014;5:211–232.
7. Amiryar ME, Pullen KR, A Review of Flywheel Energy Storage System Technologies and Their Applications. Appl Sci, 2017;7(3):286, 1-22.
8. Skinner M. Characterization of Passibe Sischarge Losses in a Flywheel Energy Storage System [Masters's Thesis], Edmonton, (AB, Canada): University of Alberta; 2017.
9. Luo X, Wang J, Dooner M, Clarke J. Overview of current development in electrical energy storage technologies and the application potential in power system operation. Appl E. 2015;137:511–536.
10. Hadjipaschalis I, Poullikkas A, Efthimiou V. Overview of current and future energy storage technologies for electric power applications. Renew Sust Energ Rev., 2009;13,1513–1522.
11. Skinner M, Mertiny P. Energy Storage Flywheel Rotors – Mechanical Design, Ency, 2022;2(1):301–324.
12. Bolund B, Bernhoff H, Leijon M, Flywheel energy and power storage systems, Renew Sust Energ Rev., 2007;11(2):235–258.
13. Łyskojć D, Duer S, Zajkowski K, Sokołowski S. Możliwości zwiększenia zasięgu pojazdu z napędem elektrycznym przy wykorzystaniu niekonwencjonalnych rozwiązań technicznych (English title.: The ability to increase the range of electric vehicle using unconventional technical solutions), Autobusy Technika, Eksploatacja, Systemy Transportowe, 2012;12(5):273–278.
14. Jansen RH, Dever TP. G2 Flywheel Module Design, NASA Technical Reports Server [Internet]. 2006, NASA/CR-2006-213862 [cited 22 May 2022]. Available from: http://large.stanford.edu/courses/2020/ph240/barnett2/docs/nasa-aug06.pdf
15. Ferrofluidowe koło zamachowe (English: Ferrofluid flywheel), KRAKsat, [Internet]. KrakSat [cited 16 Dec 2019]. Available from: https://www.kraksat.pl/space/ferrofluidowe-kolo-zamachowe/
16. Shah H. Volvo Flywheel KERS offers 25% improved economy [Internet]. 2013, article for paultan.org, [cited 16 Dec 2019]. Available from: https://paultan.org/2013/05/01/volvo-flywheel-kers-offers-25-improved-economy/
17. Chase C. Volvo Refreshes 2020 XC90 With Energy Recovery Braking System [Internet]. 2019, article for autotrader.ca, [cited 16 Dec 2019]. Available from: https://www.autotrader.ca/newsfeatures/20190222/volvo-refreshes-2020-xc90-with-energy- recovery-braking-system
18. Merksiz J, Pielecha I. Układy mechaniczne pojazdów hybrydowych (Engilsh title: Mechanical systems of hybrid vehicles). Poznań: Publishing house of Poznań University of Technology, Poznań; 2015.
19. Złoty P., Od koła garncarskiego do systemu KERS (English title: From the potter's wheel to theKERS system [Internet]. 2013, article for gazeo.pl, [cited 16 Dec 2019]. Available from: https://gazeo.pl/samochody-hybrydowe-elektryczne/samochody-hybrydowe/Od-kola-garncarskiego-do-systemuKERS,artykul,6798.html
20. Pawelskl Z, Maciejczyk A, Wróbel T. Prototype of Electric Bus of AMZ Kutno, J KONES Powertrain and Trans, 2014;21(1):197–204.
21. Szumanowski A., Akumulacja energii w pojazdach (English title: Accumulation of energy in vehicles), Warsaw: Publishing House of Communication and Connectivity, 1984.

Mateusz Kukla: https://orcid.org/0000-0003-3456-3824